




**Digital quantum simulation of the BCS model with a central-spin-like quantum processor**

Jannis Ruh <sup>\*</sup>, Regina Finsterhoelzl <sup>†</sup> and Guido Burkard <sup>‡</sup>  
*Department of Physics, University of Konstanz, D-78457 Konstanz, Germany*

 (Received 26 March 2023; accepted 18 May 2023; published 2 June 2023)

The simulation of quantum systems is one of the most promising applications of quantum computers. In this paper, we present a quantum algorithm to perform digital quantum simulations of the (reduced) Bardeen-Cooper-Schrieffer (BCS) model on a quantum register with a star-shaped connectivity map, as it is, e.g., featured by color centers in diamond. We show how to effectively translate the problem onto the quantum hardware and implement the algorithm using only the native interactions between the qubits. Furthermore, we discuss the complexity of the circuit. We use the algorithm to simulate the dynamics of the BCS model by subjecting its mean-field ground state to a time-dependent perturbation. The quantum simulation algorithm is studied using a classical simulation.

DOI: [10.1103/PhysRevA.107.062604](https://doi.org/10.1103/PhysRevA.107.062604)

**I. INTRODUCTION**

The current state of quantum computing hardware platforms has been termed the era of noisy intermediate-scale quantum (NISQ) computers [1], thereby referring to their limitations due to gate errors and decoherence effects. However, recent rapid developments may soon lead to the demonstration of advantages of useful quantum or hybrid algorithms over pure classical algorithms [2,3]. Quantum algorithms [4] have a broad area of applications, from the generalized Shor algorithm for the solution of the hidden subgroup problem [5,6] and quantum approximate optimization [7,8] to the simulation of real quantum systems [9–17]. The goal of these algorithms is to solve problems whose high computational cost makes them hard or even impossible to solve with classical hardware. Particularly, the simulation of quantum systems is among these problems due to the exponentially large dimension of the state space [18]. Since the currently available quantum hardware platforms are limited, it is important to develop implementations of quantum algorithms that make optimal use of the available hardware. To achieve this, the algorithms can be aligned with the structure of the quantum processor, i.e., with the coupling map which describes the possible connections between the qubits. Because of the limited number of available qubits and the need to protect them against decoherence and error-prone gates, it is desirable to minimize the number of operations that are required to translate the quantum algorithm to the hardware [19–24].

As small quantum systems only require a limited number of logical qubits, their simulation on the current NISQ devices has already been demonstrated for very small systems [25]. There already exist many quantum algorithms to perform such tasks [9–17]. For instance, Ref. [15] presents an algorithm that may be used to analyze the ground state and phase diagram of

the Hubbard model. However, most of the algorithms do not consider any restrictions given by the structure of the quantum hardware. This may cause the transpilation to be costly in terms of additionally needed gates.

In this paper, we present an implementation of the quantum simulation of the Bardeen-Cooper-Schrieffer (BCS) model for superconductivity. Our implementation is an example of a Hamiltonian simulation, where the quantum time evolution of a system is simulated. We will restrict the physical system to the space of Cooper pairs, which enables us to map the system efficiently onto a spin system with  $O(1)$ . This improves the performance of the algorithm; however, it also implies that the presented quantum circuit effectively simulates a spin model and not a fermionic model. To simulate the whole fermionic system, one has to use a fermionic mapping such as the Jordan-Wigner mapping [26]. While there exist analytical solutions for a time-independent system [27], our numerical quantum algorithm is applicable to the simulation of time-dependent problems and can be extended, by using trotterization techniques, to include perturbation terms. The error of the algorithm is only of a numerical nature, which can, theoretically, be reduced to be arbitrarily small. This is in contrast to analytical approximations. We restrict ourselves to the state space of paired electrons, the Cooper pairs. The algorithm is tailored to a quantum computer with a coupling map based on a central spin system (CSS). Such a quantum computer can, for instance, be realized with a spin-qubit register consisting of a nitrogen-vacancy defect in diamond [28–42]. In addition to the simulation of the BCS model, the proposed algorithm offers an efficient implementation for multiqubit gates that are double products of two-qubit gates on a CSS-like quantum register.

The paper has the following structure: In Sec. II, we introduce the physical model of a BCS superconductor, the simulated quantum system. Next we establish the connectivity map of a quantum computer based on a CSS. In Secs. III and IV, we show how to decompose the BCS Hamiltonian into CSS-like Hamiltonians and perform the mapping of the physical problem onto a quantum computer. Section V

<sup>\*</sup>jannis.ruh@uni-konstanz.de

<sup>†</sup>regina.finsterhoelzl@uni-konstanz.de

<sup>‡</sup>guido.burkard@uni-konstanz.de

describes the quantum algorithm and in Sec. VI we present our numerical results, where we simulate the time evolution of the mean-field ground state using a simulated quantum computer. We perform a quench, i.e., an abrupt parameter change in time, as a possible application of the algorithm and discuss how the algorithm can be improved.

## II. THE MODEL

The BCS theory was introduced by Bardeen, Cooper, and Schrieffer to describe the phenomenon of superconductivity through the pairing of electrons in a metal [43]. In the case of discrete states (e.g., in metallic grains) where the level spacing is of the order of the superconducting energy gap, a reduced BCS model can be used [44–46]. The Hamiltonian can then be written in the form [27,45]

$$H_{\text{BCS}} = \sum_{j=0}^{n-1} \sum_{\sigma=\uparrow,\downarrow} \epsilon_j c_{j\sigma}^\dagger c_{j\sigma} - g \sum_{j,k=0}^{n-1} c_{j\uparrow}^\dagger c_{j\downarrow}^\dagger c_{k\downarrow} c_{k\uparrow}, \quad (1)$$

where the first term corresponds to the single-particle Hamiltonian with fermionic operators  $c_{j\sigma}^\dagger$  and  $c_{j\sigma}$  describing the creation and annihilation of electrons in orbital  $j$  with energy  $\epsilon_j$  and spin  $\sigma$ , respectively. The second term describes an effective pairwise interaction between the electrons where we assume a constant and energy-level-independent coupling strength  $g$ . This coupling arises as the result of a perturbative description of the interaction between the electrons and phonons [47]. The pairing takes place between states of equal energy but antiparallel spins, i.e., between  $|j, \uparrow\rangle$  and  $|j, \downarrow\rangle$ , which occurs in a system with time-reversal invariance where the single-particle energy levels  $\epsilon_j$  are only degenerate with respect to the spin [27] or if the basis states are real wave functions. The number  $n$  of energy orbitals is assumed to be finite, for example, as in models that describe superconductivity in ultrasmall metallic grains with an energy cutoff [45,48]. Under the assumption of constant parameters  $g$  and  $\epsilon_j$ , the Hamiltonian in Eq. (1) is a well-described integrable model [49]. The BCS model given by Eq. (1) can be used to calculate the superconducting energy gap  $\Delta$ ; see Appendix B. Analytical mean-field solutions, derived with algebraic separation of variables methods [50–52], exist for its dynamics [27]. In contrast to that, the quantum algorithm to be proposed here is able to simulate the BCS system with time-dependent parameters and can be easily extended to include perturbation terms.

A central spin system can be described by a Hamiltonian of the following form [53]:

$$H_{\text{CSS}} = \sum_{j=1}^{n-1} J_j \mathbf{S}_0 \cdot \mathbf{S}_j + B \sum_{j=0}^{n-1} \mu_j S_j^z, \quad (2)$$

where  $\mathbf{S}_j = (S_j^x, S_j^y, S_j^z)^T$  are spin- $\frac{1}{2}$  operators, defined via the matrix representation  $(S_j^x, S_j^y, S_j^z)^T = \frac{\hbar}{2}(\sigma^x, \sigma^y, \sigma^z)^T$ , with the standard Pauli matrices

$$\begin{aligned} \sigma^x &= \begin{pmatrix} 0 & 1 \\ 1 & 0 \end{pmatrix}, & \sigma^y &= \begin{pmatrix} 0 & -i \\ i & 0 \end{pmatrix}, \\ \sigma^z &= \begin{pmatrix} 1 & 0 \\ 0 & -1 \end{pmatrix}. \end{aligned} \quad (3)$$

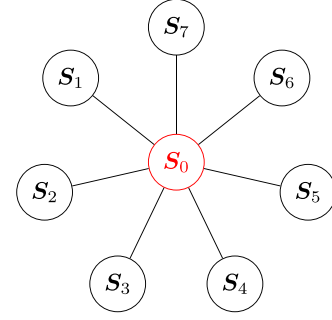


FIG. 1. The coupling map of a quantum register based on a central spin system with eight qubits. The central qubit ( $S_0$ ) is connected to all other qubits ( $S_1, \dots, S_7$ ), while the other qubits are not connected with each other.

The first term on the right-hand side of Eq. (2) represents the three-dimensional Heisenberg interaction between the spins, where the sign of the coupling constant  $J_j$  determines whether the interaction is ferromagnetic or antiferromagnetic. The interaction only appears between one central spin  $S_0$  with the surrounding spins. Thus, the connectivity map of a quantum register based on a CSS is star shaped, as shown in Fig. 1. Native two-qubit gates only exist between the central spin and the surrounding spins. This is in contrast to ideal quantum computers, where an all-to-all connectivity is assumed. The second term in Eq. (2) describes the Zeeman interaction with a magnetic field of strength  $B$  and coupling constants  $\mu_j = g_j \mu_B / \hbar$  with the Landé factor  $g_j$  and the Bohr magneton  $\mu_B$ .

## III. MAPPING ONTO A CENTRAL SPIN SYSTEM

The total Hilbert space of the considered system in Eq. (1) is given by  $\mathcal{H} = \bigotimes_{j=0}^{n-1} \mathcal{H}_j = \text{span}[\bigotimes_{j=0}^{n-1} \mathcal{B}_j]$ , with  $\mathcal{H}_j = \text{span}\mathcal{B}_j$  and the bases  $\mathcal{B}_j = \{|0\rangle, c_{j\downarrow}^\dagger |0\rangle, c_{j\uparrow}^\dagger |0\rangle, c_{j\uparrow}^\dagger c_{j\downarrow}^\dagger |0\rangle\}$ . In equal manner, we define the space of Cooper pairs  $\mathcal{H}_C = \bigotimes_{j=0}^{n-1} \mathcal{H}_{C,j}$ , with  $\mathcal{H}_{C,j} = \text{span}\mathcal{B}_{C,j}$  and  $\mathcal{B}_{C,j} = \{|0\rangle, c_{j\downarrow}^\dagger c_{j\uparrow}^\dagger |0\rangle\}$ . The orthogonal complements of  $\mathcal{H}_{C,j}$  and  $\mathcal{H}_C$  are defined via  $\mathcal{H}_{C,j}^\perp = \text{span}[\mathcal{B}_j \setminus \mathcal{B}_{C,j}]$  and  $\mathcal{H}_C^\perp = \text{span}[(\bigotimes_{j=0}^{n-1} \mathcal{B}_j) \setminus (\bigotimes_{j=0}^{n-1} \mathcal{B}_{C,j})]$ , respectively.

In order to bring the BCS Hamiltonian in connection with the Hamiltonian of a central spin system, we define the operators

$$K_j^z = \frac{1 - c_{j\uparrow}^\dagger c_{j\uparrow} - c_{j\downarrow}^\dagger c_{j\downarrow}}{2}, \quad (4)$$

$$K_j^+ = c_{j\uparrow}^\dagger c_{j\downarrow}^\dagger, \quad (5)$$

$$K_j^- = c_{j\downarrow} c_{j\uparrow}. \quad (6)$$

Here,  $K_j^z$  denotes the (shifted, negative) number operator for the  $j$ th orbital, and  $K_j^+$  ( $K_j^-$ ) creates (annihilates) a Cooper pair in the  $j$ th orbital. With these operators, one can rewrite the Hamiltonian in Eq. (1) into the following form:

$$H_{\text{BCS}} = - \sum_{j=0}^{n-1} 2\epsilon_j K_j^z - g \sum_{j,k=0}^{n-1} K_j^+ K_k^- + \text{const.} \quad (7)$$

The operators  $K_j^\alpha$  effectively represent spin- $\frac{1}{2}$  operators. Let us define the remaining components  $K_j^x = \frac{K_j^+ + K_j^-}{2}$  and  $K_j^y = \frac{K_j^- - K_j^+}{2i}$  and set  $\mathbf{K}_j = (K_j^x, K_j^y, K_j^z)^T$ . One can easily show that these operators fulfill  $\mathbf{K}_j \mathcal{H}_{C,j}^\perp = 0$  and  $\mathbf{K}_j \mathcal{H}_{C,j} \subseteq \mathcal{H}_{C,j}$ . Moreover if we map  $|0\rangle \rightarrow (1, 0)^T$  and  $\hat{c}_{j\downarrow}^\dagger \hat{c}_{j\uparrow}^\dagger |0\rangle \rightarrow (0, 1)^T$ , we find the mapping  $\mathbf{K}_j |_{\mathcal{H}_{C,j}} \rightarrow \frac{1}{2} \boldsymbol{\sigma}$ , where  $\boldsymbol{\sigma} = (\sigma^x, \sigma^y, \sigma^z)^T$  represents the vector of Pauli matrices, as in Eq. (3).

Before we map the BCS problem on a CSS-based quantum computer, we introduce the Gaudin Hamiltonians [52], a family of operators similar to a CSS Hamiltonian. For simplicity, we assume nondegenerate energy levels  $\epsilon_j$ ; however, the following can also be generalized via introducing summed-spin operators  $\tilde{\mathbf{K}}_j = \sum_{k=0}^{n-1} \mathbf{K}_k \delta_{\epsilon_j, \epsilon_k}$  and describing the BCS Hamiltonian with these operators. For  $q \in \{0, \dots, n-1\}$ , we define the Gaudin Hamiltonians as

$$H_q = 2 \sum_{\substack{j=0 \\ j \neq q}}^{n-1} \frac{\mathbf{K}_q \cdot \mathbf{K}_j}{\epsilon_q - \epsilon_j} - \gamma K_q^z, \quad (8)$$

with the free parameter  $\gamma$ . These Hamiltonians can be seen as a special case of the CSS Hamiltonian in Eq. (2), if we assume either constant  $\mu_j = \mu$  for  $j = 1, \dots, n-1$ , with a conserved total spin, or  $\mu_j \ll \mu_0$  for  $j = 1, \dots, n-1$ . The central spin is at index  $q$ . If we choose  $\gamma = -\frac{2}{g}$ , the Gaudin Hamiltonians represent a set of invariants with respect to the BCS Hamiltonian [49], i.e.,  $[H_{\text{BCS}}, H_q] = 0$  and  $[H_p, H_q] = 0$ . Moreover, we can construct the BCS Hamiltonian with them,

$$H_{\text{BCS}} = -g \sum_{q=0}^{n-1} \epsilon_q H_q + g L^z + g (L^z)^2, \quad (9)$$

where we used the total spin operator  $L$  that is defined as  $L = \sum_{j=0}^{n-1} \mathbf{K}_j$ . Note that the Gaudin Hamiltonians also fulfill  $-\gamma L^z = \sum_{q=0}^{n-1} H_q$ . If the energy levels  $\epsilon_j$  are degenerate, there is an additional term in the Hamiltonian in Eq. (9) (see Appendix A for more details) [52,54].

#### IV. MAPPING ONTO A QUANTUM COMPUTER

We restrict ourselves to the Hilbert space  $\mathcal{H}_C$  of Cooper pairs. This enables us to map the operators  $\mathbf{K}_j$  with a resource overhead of the order of  $O(1)$  onto a quantum computer. This stands in contrast to other mappings, e.g., the Jordan-Wigner mapping, which maps creation and annihilation operators to Pauli operators with an overhead of the order of  $O(n)$ , where  $n$  is the number of qubits, or the Bravyi-Kitaev mapping with a mapping of the order of  $O(\log n)$  [26]. As demonstrated in Sec. III, the space  $\mathcal{H}_C$  is invariant under the action of the operators  $\mathbf{K}_j$ . This implies that  $\mathcal{H}_C$  is also invariant under  $H_{\text{BCS}}$  [Eq. (1)] since  $H_{\text{BCS}}$  can be expressed through the spin operators as in Eq. (9). Moreover, since the Hamiltonian  $H_{\text{BCS}}$  is Hermitian, it is block diagonal with respect to  $\mathcal{H}_C$  and its complement  $\mathcal{H}_C^\perp$ . From a physical point of view, this is caused by the fact that the interaction term in Eq. (1) only rearranges the energy levels that are occupied by Cooper pairs; it does not break up or create any Cooper pairs into or out of single occupied energy levels, respectively. The block-diagonal form

enables us to consider the Hilbert space  $\mathcal{H}_C$  as a self-contained system.

The mapping onto qubits is done via

$$\prod_{j=0}^{n-1} (K_j^+)^{\beta_j} |0\rangle \rightarrow |\{q_j\}\rangle, \quad (10)$$

with  $q_j = \beta_j \in \{0, 1\}$  and

$$\mathbf{K}_j \rightarrow \frac{1}{2} \boldsymbol{\sigma}_j, \quad (11)$$

where  $|\{q_j\}\rangle = |q_{n-1} \dots q_0\rangle$  represents a basis state of the qubits on the quantum computer. Here we make use of the possibility to represent the operators  $\mathbf{K}_j$  with the Pauli operators in  $\mathcal{H}_C$ , as described in Sec. III. This mapping is similar to the proposed mapping in [55], where different kinds of pairings are investigated. Note that we do not have to consider any parity signs caused by fermionic anticommutators since the fermionic creation and annihilation operators always appear pairwise. This makes the proposed mapping more efficient than the mapping of single creation and annihilation operators.

#### V. SIMULATION

Let us first consider the case with constant parameters  $\epsilon_j$  and  $g$ , and without perturbation terms. The time-evolution operator at time  $t$  of the BCS Hamiltonian in Eq. (9), mapped onto a quantum computer as described in Sec. IV, is given by

$$U(t) = e^{-i \frac{t}{\hbar} H_{\text{BCS}}} \quad (12a)$$

$$= \left( \prod_{q=0}^{n-1} e^{i \frac{t}{\hbar} g \epsilon_q H_q} \right) \left( \prod_{\substack{j,k=0 \\ j \neq k}}^{n-1} e^{-i \frac{t}{\hbar} g \sigma_j^z \sigma_k^z / 4} \right) \times \left( \prod_{j=0}^{n-1} e^{-i \frac{t}{\hbar} g \sigma_j^z / 2} \right), \quad (12b)$$

with the Gaudin Hamiltonians

$$H_q = \sum_{\substack{j=0 \\ j \neq q}}^{n-1} \frac{\boldsymbol{\sigma}_q \cdot \boldsymbol{\sigma}_j}{2(\epsilon_q - \epsilon_j)} + \frac{\sigma_q^z}{g}. \quad (13)$$

Here we made use of the fact that in the BCS Hamiltonian, given by Eq. (9), every term commutes with all the other terms (see Appendix A). Please note that we neglect a constant phase of  $-\frac{ng}{2} + \sum_{j=0}^{n-1} \epsilon_j$  with respect to the Hamiltonian in Eq. (1). This phase would have to be taken into account, for example, if one performs a phase estimation [56] to calculate the eigenvalues of the BCS Hamiltonian and one is interested in the absolute values of the energies.

To implement the exponential operators in Eq. (12b), we define the operators

$$U_{\text{SH},jk}(\alpha) = e^{-i\alpha \sigma_j \cdot \sigma_k}, \quad U_{\text{SL},jk}(\alpha) = e^{-i\alpha \sigma_j^z \sigma_k^z}, \quad (14)$$

for a parameter  $\alpha \in \mathbb{R}$ . The exponent of the first operator  $U_{\text{SH},jk}(\alpha)$  describes a Heisenberg-type interaction, while the exponent of  $U_{\text{SL},jk}(\alpha)$  describes an Ising-type interaction. We need to implement these two-qubit operators on the quantum

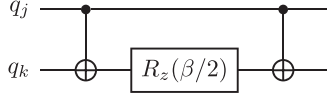


FIG. 2. Implementation of the Ising time evolution operator  $e^{-i\alpha\sigma_j^z\sigma_k^z}$ . The rotation parameter is given by  $\beta = 4\alpha$ . We do not need to perform a basis transformation, as in Fig. 3, since the evolution operator is already diagonal in the computational basis.

processor. For this, we briefly repeat the matrix representations of some standard gates. The Pauli gates are defined, accordingly with the Pauli matrices in Eq. (3), as  $X = \sigma_x$ ,  $Y = \sigma_y$ ,  $Z = \sigma_z$ . Some useful roots of the Pauli gates are

$$X^{1/2} = \frac{1}{2} \begin{pmatrix} 1+i & 1-i \\ 1-i & 1+i \end{pmatrix} = (X^{-1/2})^*, \quad (15)$$

$$S = \begin{pmatrix} 1 & 0 \\ 0 & i \end{pmatrix} = \sqrt{Z}. \quad (16)$$

The Hadamard gate and a rotation around the  $z$  axis are given by

$$H = \frac{1}{2} \begin{pmatrix} 1 & 1 \\ 1 & -1 \end{pmatrix}, \quad (17)$$

$$R_z(\lambda) = \begin{pmatrix} e^{-i\lambda/2} & 0 \\ 0 & e^{i\lambda/2} \end{pmatrix}. \quad (18)$$

The CONTROLLED-NOT gate and the SWAP gate are defined as

$$\text{CNOT}_{jk} = \begin{pmatrix} 1 & 0 & 0 & 0 \\ 0 & 0 & 0 & 1 \\ 0 & 0 & 1 & 0 \\ 0 & 1 & 0 & 0 \end{pmatrix}, \quad (19)$$

$$\text{SWAP}_{jk} = \begin{pmatrix} 1 & 0 & 0 & 0 \\ 0 & 0 & 1 & 0 \\ 0 & 1 & 0 & 0 \\ 0 & 0 & 0 & 1 \end{pmatrix}, \quad (20)$$

where the  $j$ th qubit controls the  $k$ th qubit, assuming the basis

$$|0\rangle_k|0\rangle_j = |00\rangle \leftrightarrow (1, 0, 0, 0)^T, \quad (21)$$

$$|0\rangle_k|1\rangle_j = |01\rangle \leftrightarrow (0, 1, 0, 0)^T, \quad (22)$$

$$|1\rangle_k|0\rangle_j = |10\rangle \leftrightarrow (0, 0, 1, 0)^T, \quad (23)$$

$$|1\rangle_k|1\rangle_j = |11\rangle \leftrightarrow (0, 0, 0, 1)^T. \quad (24)$$

With these gates, it is possible to implement  $U_{\text{SH},jk}(\alpha)$  and  $U_{\text{sl},jk}(\alpha)$  in Eq. (14), as shown in Figs. 2 and 3. Figure 3 shows a general approach to construct gates with an action  $e^{iA}$  for a Hermitian operator  $A$  by implementing the basis transformation from the eigenbasis of  $A$  to the  $z$  basis, followed by  $z$  rotations according to the eigenvalues of  $A$  and a back transformation from the  $z$  basis to the eigenbasis. For example, in the case of  $U_{\text{SH},jk}$ , the operator  $\sigma_j \cdot \sigma_k$  is diagonal in the Bell basis,

$$|\phi_{\pm}\rangle = \frac{|00\rangle \pm |11\rangle}{\sqrt{2}}, \quad |\psi_{\pm}\rangle = \frac{|01\rangle \pm |10\rangle}{\sqrt{2}}, \quad (25)$$

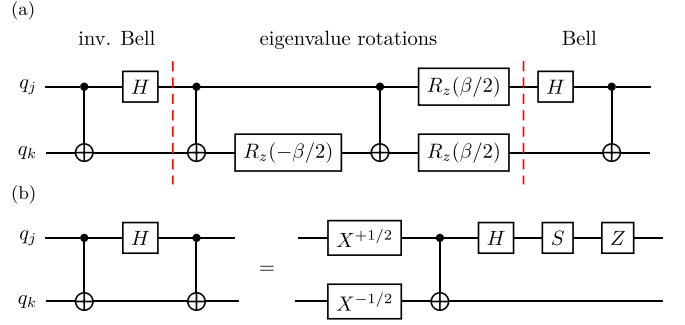


FIG. 3. From Ref. [57]. (a) Implementation of the Heisenberg time-evolution operator  $e^{-i\alpha\sigma_j \cdot \sigma_k}$ . The rotation parameter is given by  $\beta = 4\alpha$ . First the Bell basis, as defined in Eq. (25) (the eigenvectors of  $\sigma_j \cdot \sigma_k$ ), is mapped to the  $z$  basis; then  $z$  rotations, according to the eigenvalues ( $+1$  for  $|\phi_{\pm}\rangle$ ,  $|\psi_{+}\rangle$  and  $-3$  for  $|\psi_{-}\rangle$ ), are executed; and, in the end, the  $z$  basis is mapped back to the Bell basis. (b) Implementation of the first three gates in (a) to replace one CNOT.

with the eigenvalue  $+1$  for  $|\phi_{\pm}\rangle$ ,  $|\psi_{+}\rangle$  and  $-3$  for  $|\psi_{-}\rangle$ . Therefore we map, as described in Fig. 3 (see, also, [57]),

$$(|\phi_{+}\rangle, |\phi_{-}\rangle, |\psi_{+}\rangle, |\psi_{-}\rangle) \quad (26a)$$

$$\mapsto (|00\rangle, |01\rangle, |10\rangle, |11\rangle) \quad (26b)$$

$$\mapsto (e^{-i\alpha}|00\rangle, e^{-i\alpha}|01\rangle, e^{-i\alpha}|10\rangle, e^{3i\alpha}|11\rangle) \quad (26c)$$

$$\mapsto (e^{-i\alpha}|\phi_{+}\rangle, e^{-i\alpha}|\phi_{-}\rangle, e^{-i\alpha}|\psi_{+}\rangle, e^{3i\alpha}|\psi_{-}\rangle). \quad (26d)$$

$U_{\text{sl},jk}$  is already diagonal in the  $z$  basis, so we can directly perform the  $z$  rotations, as described in Fig. 2,

$$(|00\rangle, |01\rangle, |10\rangle, |11\rangle) \quad (27a)$$

$$\rightarrow (e^{-i\alpha}|00\rangle, e^{i\alpha}|01\rangle, e^{i\alpha}|10\rangle, e^{-i\alpha}|11\rangle). \quad (27b)$$

The evolution of

$$U(H_q, t) = e^{i\frac{t}{\hbar}g\epsilon_q H_q} \quad (28)$$

can be approximated using the Trotter-Suzuki formulas [58,59], which factorize the exponential operator. The first-order and second-order Trotter-Suzuki formulas for two noncommuting operators  $A$  and  $B$  are given by, respectively,

$$e^{it(A+B)} = \lim_{m \rightarrow \infty} (e^{iA\Delta t} e^{iB\Delta t})^m, \quad (29)$$

$$e^{it(A+B)} = \lim_{m \rightarrow \infty} (e^{iB\Delta t/2} e^{iA\Delta t} e^{iB\Delta t/2})^m, \quad (30)$$

with the discrete time step  $\Delta t = \frac{t}{m}$ . For finite  $m$ , the errors  $\varepsilon_1, \varepsilon_2$ , for the first and second order, respectively, have the upper bound

$$\varepsilon_1 \leq \frac{t^2}{2m} \| [A, B] \| + O\left(\frac{t^3}{m^3}\right), \quad (31)$$

$$\varepsilon_2 \leq \frac{t^3}{12m^2} \left\| \left[ A + \frac{B}{2}, [A, B] \right] \right\| + O\left(\frac{t^4}{m^4}\right). \quad (32)$$

Using the formulas in Eqs. (29) and (30), we decompose  $U(H_q, t)$  into terms of single rotations around the  $z$  axis and  $U_{\text{SH},qj}$  [Eq. (14)]. With this given, the time evolution  $U(t)$  is easily implemented on an ideal quantum register with an all-to-all connectivity. However, such ideal quantum computers are not realistic.

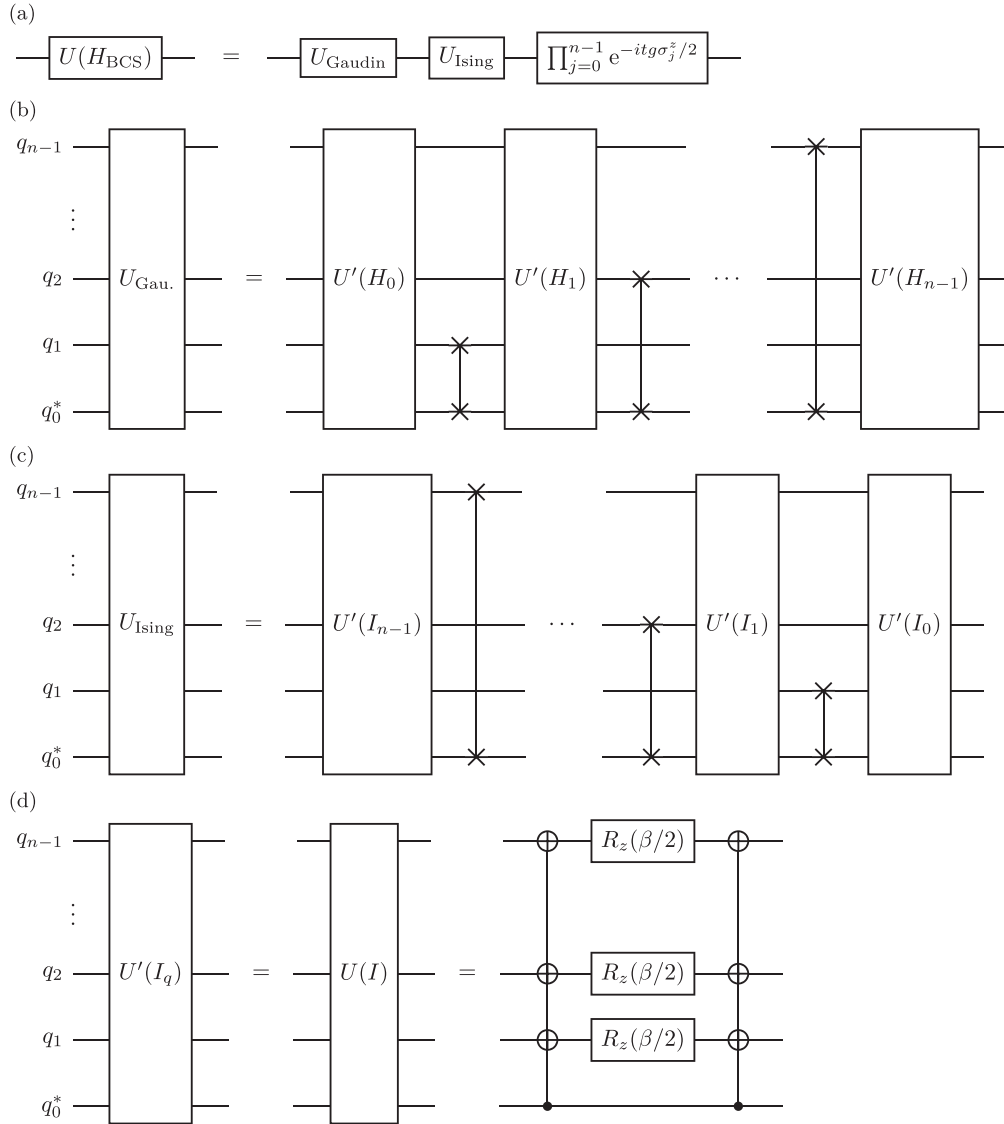


FIG. 4. Implementation of the BCS time evolution  $U(t) = U(H_{\text{BCS}})$  for constant parameters on a CSS quantum register. The lowest wire represents the central qubit  $q_0^*$ . (a) Decomposition of the BCS evolution into a Gaudin term, an Ising term, and some single-qubit rotations. (b) Implementation of the Gaudin term (multiple Gaudin Hamiltonians). The operators  $U'(H_j) = U(H_0, t)[\{\epsilon_{j,k}\}_k, g]$  are recursively defined via Eq. (28) and  $\{\epsilon_{j,k}\}_k = h_{j,0}(\{\epsilon_{j-1,k}\}_k)$  for  $j > 0$  and  $\{\epsilon_{0,k}\}_k = \{\epsilon_k\}_k$ , where  $h_{j,m}$  swaps the elements  $a_j$  and  $a_m$  in a tuple  $\{a_k\}$ .  $U(H_0, t)$  can, for example, be implemented with the Trotter-Suzuki formulas. (c) The Ising term evolution. Note that this gate inverts the qubit permutations from the Gaudin gate. (d) Implementation of one of the Ising gates with  $\beta = tg$ . Note that the single-qubit gates do not depend on  $q$ .

We consider the case of a CSS quantum register with a star-shaped connectivity map as described in Sec. II. Let  $q_0^*$  be the central qubit that couples to all other qubits. To implement the time evolution, we make use of the SWAP gate. The algorithm is visualized in Fig. 4. First, we implement  $U(H_0, t)$  which only contains couplings with the central qubit  $q_0^*$ . Next we perform a SWAP operation on the qubits  $q_0^*$  and  $q_1$ . Now we can implement  $U(H_1, t)$  with adapted parameters as described in Fig. 4(b). Next we swap the states on the qubits  $q_0^*$  and  $q_2$  and proceed in the same manner until we reach the last qubit. This procedure implements the first term  $\prod_{q=0}^{n-1} e^{i\frac{t}{\hbar} g \epsilon_q H_q}$  in Eq. (12b), however with swapped states at the end. This will be fixed with the second term in Eq. (12b). For

this, we define the operators  $U(I_q, t) = \prod_{j=0; j \neq q}^{n-1} e^{-i\frac{t}{\hbar} g \sigma_q^z \sigma_j^z/4}$ . With these operators, we proceed analog as with the Gaudin terms  $U(H_q, t)$ , however starting with the  $(n-1)$ th qubit, i.e., starting with  $U(I_{n-1}, t)$ , as described in Fig. 4(c).

While the exact total number of required gates depends on the given set of native gates, the complexity, i.e., the gate count of the algorithms with respect to the number of qubits,  $n$ , is of great interest.  $U(H_q, t)$  is implemented using the Trotter-Suzuki formula by splitting the evolution into  $r_q(t, \epsilon, \{\epsilon_j\}, g) \cdot n$  exponential operators, where the operators are either  $U_{\text{SH},jk}(\alpha)$  or single qubit rotations around the  $z$  axis. The factor  $r_q(t, \epsilon, \{\epsilon_j\}, g)$  depends on the chosen Trotter-Suzuki decomposition, where  $\epsilon$  is the error of the

approximation. For example, a  $2p$ th order Trotter-Suzuki decomposition exists where

$$r_q(t, \varepsilon, \{\epsilon_j\}, g) \approx O\left(\frac{p25^p}{3^{p-1}} \sqrt[2p]{\frac{(\Lambda_q(\{\epsilon_j\}, g)t)^{2p+1}}{\varepsilon}}\right) \quad (33)$$

can be reached [58–61]. For the BCS problem, one finds that  $\Lambda_q(\{\epsilon_j\}, g)\hbar = \sum_{j=0}^{n-1} |\frac{3g\epsilon_q}{2\epsilon_q - \epsilon_j}| + |\epsilon_q|$ . However, this value is only an estimate which provides an upper bound of the number of needed gates, and smaller  $r_q(t, \varepsilon, \{\epsilon_j\}, g)$  may be possible. It follows that the algorithm, as proposed in Fig. 4, has a maximum circuit-size complexity of  $O(\max_q(r_q(t, \varepsilon, \{\epsilon_j\}, g))^n)$ , both in terms of single-qubit and two-qubit gates. The circuit-depth complexity is of the same order. This means that up to the factor  $\max_q(r_q(t, \varepsilon, \{\epsilon_j\}, g))$ , the complexity is quadratic in the number of qubits. However, the dependence of  $\max_q(r_q(t, \varepsilon, \{\epsilon_j\}, g))$  on the system parameters  $\epsilon_j$  and  $g$  and the time  $t$  is not trivial in general.

The algorithm demonstrates that CSS quantum registers represent a powerful platform when it comes to the implementation of double products of two-qubit gates. Let us consider the operator  $f = \prod_{j \in M} \prod_{k \in S_j} f_{jk}$ , where  $f_{jk}$  is a unitary operator on the qubits  $j$  and  $k$ , for the tuples  $(M_j)_j, (S_{j,k})_k \subset \{0, \dots, n-1\}$ , where  $j = 1, \dots, |M|$ . This operator is a product of operators  $\hat{S}_j = \prod_{k \in S_j} f_{jk}$ , where each of these operators has effectively one central “spin” that needs to interact with all the other “spins.” On a CSS quantum register, the operators  $\hat{S}_j$  can be implemented successively by swapping the central qubit with the  $j$ th qubit in between and adapting the parameters in an analog way as in Fig. 4(b). With this, the number of necessary SWAPgates for the implementation  $f$  is of the order of  $O(|M|)$ , where  $|M|$  counts the number of times where the role of the central spin changes. The trivial special case,  $|M| = 1$ , can, for example, be used to simulate the central-spin system itself, which has application in solving nonlinear differential equations [62].

The algorithm for the time-independent BCS Hamiltonian in Eq. (9), that we have shown above, can be easily expanded by using the same trotterization techniques that we have already used, to a more general time-dependent Hamiltonian including possible perturbations

$$H(t) = H_{\text{BCS}}(t) + H_{\text{P}}[\{\mathbf{K}_j\}](t), \quad (34)$$

where the perturbation term  $H_{\text{P}}[\{\mathbf{K}_j\}](t)$  needs to be expressible only using the spin operators  $\{\mathbf{K}_j\}$ , so that the mapping in Sec. IV is applicable. The time-evolution operator is given by the Dyson series,

$$U(t, t_0) = \mathcal{T}\left[e^{-\frac{i}{\hbar} \int_{t_0}^t H(t') dt'}\right], \quad (35)$$

where  $\mathcal{T}$  is the time-ordering operator. To simulate the time evolution up to the time  $t$ , one can discretize the total time  $t - t_0$  into  $m$  steps and split the time-evolution operator as follows:

$$U(t, t_0) = U(t = t_m, t_{m-1}) \dots U(t_1, t_0), \quad (36)$$

where the operators  $U(t_j, t_{j-1})$  can be approximated with

$$U(t_j, t_{j-1}) \approx e^{-\frac{i}{\hbar} H(t_{j-1}) \Delta t_{j,j-1}}, \quad (37)$$

if the chosen time difference  $\Delta t_{j,j-1} = t_j - t_{j-1}$  is sufficiently small. The operators  $U(t_j, t_{j-1})$  can be approximated using the Trotter-Suzuki decompositions and the implementation for the BCS evolution from the constant case.

## VI. RESULTS

In this section, we present our numerical results for the simulation of the dynamics of the model and discuss further optimization strategies and application fields. The numerical calculations are performed with a simulated quantum computer. As a test for the proper function of the quantum simulation, we calculate the return probability, i.e., the probability that the system after time  $t$  [described by the state vector  $|\psi(t)\rangle$ ] has returned to its initial state  $|\psi_0\rangle$ ,

$$|\langle\psi_0|\psi(t)\rangle|^2 = |\langle\psi_0|\mathcal{T}\left[e^{-\frac{i}{\hbar} \int_{t_0}^t H_{\text{BCS}}(t') dt'}\right]|\psi_0\rangle|^2. \quad (38)$$

Note that the return probability equals the Loschmidt echo, which constitutes an important quantity in multiple contexts of the quantum many-body theory, for example, quantum chaos and nonequilibrium fluctuation theorems [63,64]. Here, we assume a Hamiltonian  $H_{\text{BCS}}(t)$  as in Eq. (9) with time-dependent parameters. As the initial state, we use  $|\psi_0\rangle = |\text{BCS}\rangle$ , where  $|\text{BCS}\rangle$  is the ground state of the mean-field BCS theory at time  $t_0$ , given as

$$|\text{BCS}\rangle = \prod_{j=0}^{n-1} (u_j - v_j K_j^+) |0\rangle. \quad (39)$$

The parameters  $u_j, v_j \in \mathbb{C}$  depend on the system parameters  $\epsilon_k(t_0)$  and  $g(t_0)$ ; for details, see Appendix B and Ref. [65]. Since  $|\text{BCS}\rangle \in \mathcal{H}_{\text{C}}$ , the problem is suitable for the algorithm presented above. For a constant Hamiltonian, the state  $|\text{BCS}\rangle$  approximates the ground state for  $n \rightarrow \infty$ , implying that the return probability in Eq. (38) approaches 1. Because of its form of a product state,  $|\text{BCS}\rangle$  can be easily implemented using single-qubit rotations.

In the presence of errors, a quantum simulation is not perfect; rather, the simulation results in a mixed state, which can be described with a density matrix  $\rho(t)$ . Therefore, instead of the return probability as in Eq. (38), we actually calculate

$$\mathcal{R}_{\text{mf}}(t) = \langle 0 | \rho_{\text{mf}}(t) | 0 \rangle. \quad (40)$$

The density matrix  $\rho_{\text{mf}}$  is the result of the quantum simulation, which consists of initializing the mean-field ground state  $|\text{BCS}\rangle$ , performing the time evolution, and inverting the mean-field ground-state initialization. All these operations might be error prone. In the optimal case, without any errors, the density matrix describes the following pure state:

$$\rho_{\text{mf}}^{\text{opt}}(t) = |\phi_{\text{mf}}(t)\rangle \langle \phi_{\text{mf}}(t)|, \quad (41)$$

$$|\phi_{\text{mf}}(t)\rangle = \langle \psi_{\text{mf},0} | \psi_{\text{mf}}(t) \rangle |0\rangle + \sqrt{1 - |\langle \psi_{\text{mf},0} | \psi_{\text{mf}}(t) \rangle|^2} |0^\perp\rangle, \quad (42)$$

where  $|0^\perp\rangle$  is a state orthogonal to  $|0\rangle$ .  $|\psi_{\text{mf},0}\rangle$  and  $|\psi_{\text{mf}}(t)\rangle$  are the state  $|\text{BCS}\rangle$  and its time-evolved state, respectively. In this optimal case,  $\mathcal{R}_{\text{mf}}(t)$  equals the formula in Eq. (38).

In addition to the simulation of the mean-field ground state, we calculate the return probability for the exact ground state

of the Hamiltonian in Eq. (9). However, we do not implement the initialization of this state in the quantum algorithm; instead, we directly specify this state as the initial state. This is only possible because we use a simulated quantum computer and not a real quantum device. The resulting quantity of the simulation is the return probability,

$$\mathcal{R}_{\text{exact}}(t) = \langle \psi_{\text{exact},0} | \rho_{\text{exact}}(t) | \psi_{\text{exact},0} \rangle, \quad (43)$$

where, in the optimal case, without qubit and gate errors, the density matrix  $\rho_{\text{exact}}(t)$  describes the state

$$\rho_{\text{exact}}^{\text{opt}}(t) = |\psi_{\text{exact}}(t)\rangle \langle \psi_{\text{exact}}(t)|. \quad (44)$$

Here,  $|\psi_{\text{exact},0}\rangle$  and  $|\psi_{\text{exact}}(t)\rangle$  are the exact ground state, at time  $t_0$ , and its time-evolved state, respectively.

A quantum quench describes the process of initializing a system in a certain state, often an eigenstate, e.g., the ground state, and subjecting the system to a time-dependent modification of parameters or, for example, a perturbation [63,67,68]. We simulate a quench, varying the superconducting gap  $\Delta$ , realized via a change of the coupling constant  $g$ . After some time, the quench is performed backwards, i.e.,  $g$  is reset to its initial value.

We introduce a dimensionless time  $\tau(t) = \frac{t\tilde{\mathcal{J}}}{\hbar}$ , where  $\tilde{\mathcal{J}}$  is an arbitrary energy unit. Without loss of generality, we set  $t_0 = 0$ . The classical simulation of our quantum circuit is done for  $n = 5$  qubits. For the energy levels, we choose a harmonic oscillator, i.e.,  $\epsilon_j = \omega(j + \frac{1}{2})$ , as one of the simplest noninteracting systems. The coupling strength  $g$  is time dependent, according to

$$g(t) = \frac{(g_c - g_0)}{\pi^2} \left[ \arctan\left(\frac{(t - t_1)\tilde{\mathcal{J}}}{\hbar\Gamma}\right) + \frac{\pi}{2} \right] \times \left[ \arctan\left(\frac{(t_2 - t)\tilde{\mathcal{J}}}{\hbar\Gamma}\right) + \frac{\pi}{2} \right] + g_0, \quad (45)$$

which is plotted in Fig. 5(a). The parameter  $\Gamma$  describes the smoothness of the quench and  $t_1$  and  $t_2$  are the times when the quench and the reverse quench take place, respectively.  $g_0$  is the initial coupling constant and  $g_c$  is the coupling constant after the quench. The results of the numerical simulation are depicted in Fig. 5. The chosen set of parameters is given by  $t_1 = 9\hbar/\tilde{\mathcal{J}}$ ,  $t_2 = 18\hbar/\tilde{\mathcal{J}}$ ,  $\Gamma = 0.1$ , and  $\omega = \frac{5}{3}\tilde{\mathcal{J}}$ , while  $g_0$  and  $g_c$  are calculated from the superconducting gaps  $\Delta_0 = \tilde{\mathcal{J}}$  and  $\Delta_c = 2\tilde{\mathcal{J}}$ , respectively [details are given in Appendix B, Eq. (B9)]. For all our simulations, we remain at zero temperature,  $T = 0$  K. The trotterization of the Gaudin Hamiltonians is performed using the first- and second-order equations from Eqs. (29) and (30), where we specified the error  $\epsilon_1$  in Eq. (31) to be smaller than  $\frac{3}{5}C$ , where  $C$  is the constant factor caused by the noncommuting terms in the Gaudin Hamiltonians, i.e., we set the number of Trotter steps to  $m(\tau) \approx \frac{5}{6}\tau^2$ . This is only an approximation because the Trotter step width  $\tau/m(\tau)$  has to be adapted to the splitting of the Dyson series, which depends dynamically on the system parameters in our simulation. With that, we can count the number of CNOTs in our quantum circuit: There are  $2(n - 1)$  SWAP gates where each can be decomposed into three alternating CNOTs. We have  $n$  Gaudin terms, where each of them is trotterized with  $m(\tau)$  steps; each step contains  $n - 1$  Heisenberg evolution operators as in Fig. 3 (first-order trotterization), which require three CNOTs.

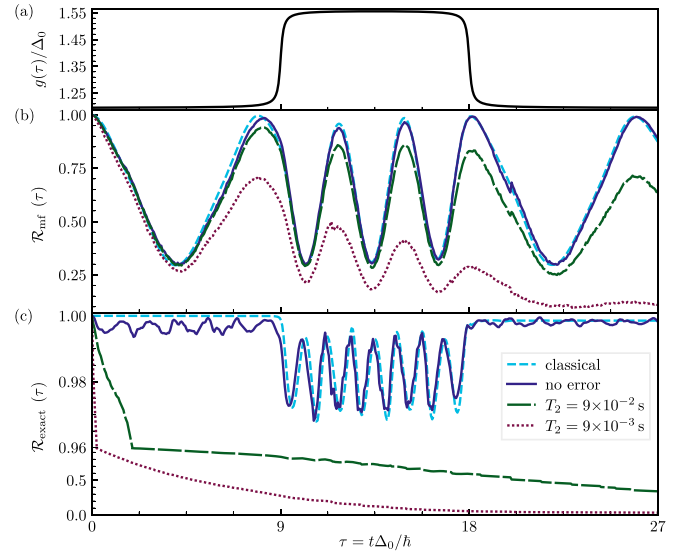


FIG. 5. The time-dependent return probability  $\mathcal{R}(t)$  of a state  $|\psi(t)\rangle$  to its initial state  $|\psi_0\rangle$  ( $t_0 = 0$ ), where the state  $|\psi(t)\rangle = \mathcal{T}[\exp(-\frac{i}{\hbar} \int_{t_0}^t H_{\text{BCS}}(t') dt')] |\psi_0\rangle$  describes the time evolution, determined by the BCS Hamiltonian in Eq. (9). (a) The time-dependent coupling function  $g(\tau) := g(t(\tau))$  as defined in Eq. (45). (b) The return probability  $\mathcal{R}_{\text{mf}}(t) := \mathcal{R}_{\text{mf}}(t(\tau))$ , described in (40–42), for the mean-field ground state  $|\text{BCS}\rangle$ , defined in Eq. (39), as the initial state. (c) The return probability  $\mathcal{R}_{\text{exact}}(t) := \mathcal{R}_{\text{exact}}(t(\tau))$ , as described in Eqs. (43) and (44), for the exact ground state of the BCS Hamiltonian in Eq. (9) as the initial state. In both (b) and (c), the results are calculated with a simulated quantum computer provided by Ref. [66]. The dark-blue solid line shows the return probability, calculated with the quantum algorithm under the assumption of error-free qubits and gates, and the light-blue dashed line is the classical calculated return probability (“classical” in the sense that a classical algorithm with high precision is used). Up to numerical errors, caused by the trotterization, these lines are the same. The green long-dashed line and the red-magenta dotted line are the results of the quantum simulation with noisy qubits, but without gate errors, i.e., the execution of the gates is assumed to be error free, however, the qubit errors can still spread from one qubit to another. As for the qubit error, we model transversal and longitudinal relaxation based on an amplitude-phase-damping channel with the coherence times  $T_1 = 1.25 \times 10^{-1}$  s,  $T_2 = 9 \times 10^{-2}$  s (green long-dashed),  $T_2 = 9 \times 10^{-3}$  s (magenta-red dotted), a single-qubit gate time  $t_s = 5 \times 10^{-8}$  s, and a two-qubit gate time  $t_r = 5 \times 10^{-7}$  s. We do not consider any coherent or crosstalk errors.

There are  $n$  Ising terms and each of them contains  $n - 1$  Ising evolution operators as in Fig. 2 with two CNOTs. Summing things up, the total number of CNOTs is as follows:

$$N_{\text{CNOT}}(\tau) = 6(n - 1) + 3n(n - 1)m(\tau) + 2n(n - 1) \quad (46a)$$

$$= 2n^2 + 4n - 1 + \frac{5}{2}(n^2 - n)\tau^2 \quad (46b)$$

$$= 69 + 50\tau^2. \quad (46c)$$

In the last step, we substituted  $n = 5$ . If we insert the largest simulation time in Fig. 5,  $\tau = 27$ , we have 36 519 CNOT gates. Similar counting can be performed for the single-qubit gates.

Figure 5 shows the results of our simulations. The simulations are performed with and without qubit errors, however

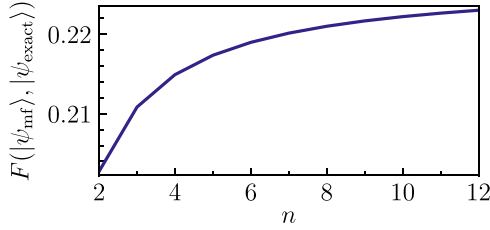


FIG. 6. The fidelity  $F$  between the mean-field ground state  $|\psi_{\text{mf}}\rangle$  and the exact ground state  $|\psi_{\text{exact}}\rangle$  as a function of the number of orbitals,  $n$ . Note that for pure states the fidelity equals the squared absolute value of the scalar product,  $F = |\langle\psi_{\text{mf}}|\psi_{\text{exact}}\rangle|^2$ . In this case,  $F$  is time independent if the states are subject to the same time evolution.

always with perfect gates. The qubit errors are modeled with an amplitude-phase-damping channel. To compare the results, we additionally plotted the results from a classical algorithm, which is based on the diagonalization of the Hamiltonian at multiple time steps. The perfect quantum simulations, without qubit errors, lead to the same results as the classical algorithm, up to trotterization errors.

In the plotted regime, the mean-field ground state is apparently not a good approximation of the exact ground state, but this is not unexpected since we only consider five energy orbitals. Figure 6 shows the fidelity between the mean-field ground state and the exact ground state as a function of the orbital number  $n$  for the chosen system parameters. For  $n = 5$ , the fidelity is approximately 0.217363. The very small gradient of the fidelity in Fig. 6 indicates that the mean-field approximation does not perform very well for the chosen system parameters regarding the approximation of the exact ground state. This may be partly explained by the fact that the  $|\text{BCS}\rangle$  state can be considered as a solution of a variation ansatz minimizing the energy expectation value. This means that while the energy expectation value of  $|\text{BCS}\rangle$  approximates the ground-state energy fairly well, the state itself may not approximate the ground state similarly well if there is some other eigenstate that has an energy near to the ground-state energy. This justifies the use of the exact ground state in our simulations.

The curves that are simulated with noisy qubits deviate strongly from the perfect simulation. These deviations increase with time  $t$  since more gates are needed and therefore the duration of the computation increases. This increases the effect of the qubit relaxation errors. In the case of the exact ground state, the relative differences between the extrema are so small that it is difficult to resolve any qualitative behavior if we consider the qubit noise.

To improve the algorithmic performance for longer times  $t$ , one has to minimize the number of needed gates. One approach is to optimize the choice of the time steps in Eq. (36). In areas where  $g(t) \approx \text{const}$ , the time step  $\Delta t_{j,j-1}$  can be bigger than in areas where  $g(t)$  is changing fast. We chose the time steps depending only on the first and second derivative of  $g(t)$  in a similar manner to gradient descent methods, i.e., we made a “big” time step if both the first and second derivatives were “small,” and vice versa. However, this approach

does not directly reduce the number of needed gates for the trotterization. This may be reached by using higher-order Trotter-Suzuki formulas; however, please note that the optimal order depends on the time, e.g., as in Eq. (33), and it is even more difficult to find the optimal order if the system parameters vary over time. In the present paper, we used first- and second-order formulas as given in Eqs. (29) and (30). Another more hardware-specific optimization would be to implement the circuit using only native gates and, if possible, using the ones with the smallest errors, i.e., helping the transpiler to find the best circuit. One can also try to trotterize  $U(H_q, t)$  into gates including more than two qubits. We used the two-qubit gate described in Fig. 3 and a rotation around the  $z$  axis.

## VII. CONCLUSION

Our work provides a quantum algorithm capable of simulating the time-dependent BCS model. We restricted ourselves to the space of Cooper pairs, which enabled us to map the physical problem very efficiently with order  $O(1)$  onto a quantum register, in contrast, for example, to the Jordan-Wigner mapping. The algorithm exploits invariants of the BCS system, i.e., we expressed the Hamiltonian with the commuting Gaudin Hamiltonians. Furthermore, we used the structure of the Gaudin Hamiltonians to implement the algorithm on a quantum register with a star-shaped coupling map, only making use of its native connectivity. Additionally, we demonstrated that this algorithm provides a general effective method to implement double products of two-qubit operators on such a quantum register. Finally, we showed some numerical results, simulating a quenched time evolution of the mean-field ground state, and proposed possible optimizations for future work. Further alternative methods, which might be interesting to improve the performance of the algorithm, such as simulating the time evolution via truncating the Taylor series of the time-evolution exponential, are proposed in Refs. [69,70]. The simulation results with quantum errors indicate that quantum error correction and/or better quantum hardware will be needed to perform real quantum simulations with valuable results. For example, it has been shown that crosstalk errors can be mitigated with an appropriate algorithm [71]. Apart from simulating the time evolution, a possible extension of our proposed algorithm is the calculation of the eigenvalues of the BCS Hamiltonian via (hybrid) quantum phase estimation [56], which makes use of a controlled time evolution (see Appendix C).

## ACKNOWLEDGMENT

We acknowledge funding from the state of Baden-Württemberg through the Kompetenzzentrum Quantum Computing, Project QC4BW.

## APPENDIX A: PROPERTIES OF THE GAUDIN HAMILTONIANS

If not otherwise noted, sums over Latin indices (e.g.,  $j, k, p, q$ ) run from 0 to  $n - 1$ , while sums over Greek indices (e.g.,  $\alpha, \beta, \gamma$ ) assume the values  $x, y, z$ .



*Theorem 1.* The Gaudin Hamiltonians commute with each other, i.e.,  $[H_q, H_p] = 0$  [54].

*Proof.* Let  $q \neq p$ . We calculate the commutator separated in three steps. Let us start with the commutator of the last terms and the commutator of the mixed terms,

$$[K_q^z, K_p^z] = 0, \quad (\text{A1})$$

$$\left[ K_q^z, \sum_{j \neq p} \frac{\mathbf{K}_p \cdot \mathbf{K}_j}{\epsilon_p - \epsilon_j} \right] + \left[ \sum_{k \neq q} \frac{\mathbf{K}_q \cdot \mathbf{K}_k}{\epsilon_q - \epsilon_k}, K_p^z \right] = \left[ K_q^z, \frac{\mathbf{K}_p \cdot \mathbf{K}_q}{\epsilon_p - \epsilon_q} \right] + \left[ \frac{\mathbf{K}_q \cdot \mathbf{K}_p}{\epsilon_q - \epsilon_p}, K_p^z \right] \quad (\text{A2a})$$

$$= \frac{1}{\epsilon_p - \epsilon_q} [K_q^z + K_p^z, \mathbf{K}_p \cdot \mathbf{K}_q] \quad (\text{A2b})$$

$$= 0. \quad (\text{A2c})$$

Next is the commutator of the first terms (the intermediate steps are explained below):

$$\left[ \sum_{j \neq p} \frac{\mathbf{K}_p \cdot \mathbf{K}_j}{\epsilon_p - \epsilon_j}, \sum_{k \neq q} \frac{\mathbf{K}_q \cdot \mathbf{K}_k}{\epsilon_q - \epsilon_k} \right] = \sum_{\alpha\beta} \sum_{j \neq p} \sum_{k \neq q} \frac{[K_p^\alpha K_j^\alpha, K_q^\beta K_k^\beta]}{(\epsilon_p - \epsilon_j)(\epsilon_q - \epsilon_k)} \quad (\text{A3a})$$

$$= \sum_{\alpha\beta\gamma} i\epsilon^{\alpha\beta\gamma} \left\{ \sum_{j \neq p, q} \frac{K_p^\alpha K_q^\beta K_j^\gamma}{(\epsilon_p - \epsilon_j)(\epsilon_q - \epsilon_j)} + \sum_{j \neq q} \frac{K_p^\alpha K_q^\gamma K_j^\beta}{(\epsilon_p - \epsilon_q)(\epsilon_q - \epsilon_j)} + \sum_{j \neq p} \frac{K_q^\beta K_p^\gamma K_j^\alpha}{(\epsilon_p - \epsilon_j)(\epsilon_q - \epsilon_p)} \right\} \quad (\text{A3b})$$

$$= \sum_{\alpha\beta\gamma} \sum_{j \neq p, q} i\epsilon^{\alpha\beta\gamma} \left\{ \frac{K_p^\alpha K_q^\beta K_j^\gamma}{(\epsilon_p - \epsilon_j)(\epsilon_q - \epsilon_j)} + \frac{K_p^\alpha K_q^\gamma K_j^\beta}{(\epsilon_p - \epsilon_q)(\epsilon_q - \epsilon_j)} + \frac{K_q^\beta K_p^\gamma K_j^\alpha}{(\epsilon_p - \epsilon_j)(\epsilon_q - \epsilon_p)} \right\} \quad (\text{A3c})$$

$$= \sum_{\alpha\beta\gamma} \sum_{j \neq p, q} i\epsilon^{\alpha\beta\gamma} K_p^\alpha K_q^\beta K_j^\gamma \left\{ \frac{1}{(\epsilon_p - \epsilon_j)(\epsilon_q - \epsilon_j)} - \frac{1}{(\epsilon_p - \epsilon_q)(\epsilon_q - \epsilon_j)} - \frac{1}{(\epsilon_p - \epsilon_j)(\epsilon_q - \epsilon_p)} \right\} \quad (\text{A3d})$$

$$= 0. \quad (\text{A3e})$$

In Eq. (A3a)  $\rightarrow$  Eq. (A3b), we used

$$[K_p^\alpha K_j^\alpha, K_q^\beta K_k^\beta] = K_p^\alpha K_q^\beta [K_j^\alpha, K_k^\beta] + K_p^\alpha [K_j^\alpha, K_q^\beta] K_k^\beta + K_q^\beta [K_p^\alpha, K_k^\beta] K_j^\alpha + [K_p^\alpha, K_q^\beta] K_k^\beta K_j^\alpha \quad (\text{A4a})$$

$$= \sum_{\gamma} i\epsilon^{\alpha\beta\gamma} (\delta_{j,k} K_p^\alpha K_q^\beta K_j^\gamma + \delta_{j,q} K_p^\alpha K_j^\gamma K_k^\beta + \delta_{p,k} K_q^\beta K_k^\gamma K_j^\alpha), \quad (\text{A4b})$$

with the Levi-Civita symbol  $\epsilon^{\alpha\beta\gamma} = 1$  if  $(\alpha, \beta, \gamma) = (x, y, z)$ , cyclical, and otherwise  $\epsilon^{\alpha\beta\gamma} = -1$ . In Eq. (A3b)  $\rightarrow$  Eq. (A3c), we used that in the last two sums, the terms for  $j = p$  and  $j = q$ , respectively, cancel each other since, for  $|\{\alpha, \beta, \gamma\}| = 3$  (fix  $\gamma$  and exchange  $\alpha$  and  $\beta$ ),

$$K_p^\alpha K_q^\gamma K_p^\beta + K_q^\beta K_p^\gamma K_q^\alpha - K_p^\beta K_q^\gamma K_p^\alpha - K_q^\alpha K_p^\gamma K_q^\beta \propto K_q^\gamma K_p^\gamma - K_p^\gamma K_q^\gamma = 0. \quad (\text{A5})$$

Equation (A3c)  $\rightarrow$  Eq. (A3d) follows from permuting the indices  $\alpha, \beta, \gamma$  and adapting the signs. Finally, Eq. (A3d)  $\rightarrow$  Eq. (A3e) is valid since the term in the braces equals zero. ■

*Lemma 1.* The sum of the Gaudin Hamiltonians is proportional to the  $z$  component of the total angular momentum, i.e.,  $-\gamma L^z = \sum_q H_q$  [52].

*Proof.*

$$\sum_q H_q + \gamma L^z = 2 \sum_q \sum_{j \neq q} \frac{\mathbf{K}_q \cdot \mathbf{K}_j}{\epsilon_q - \epsilon_j} \quad (\text{A6a})$$

$$= \sum_{\substack{q,j \\ j \neq q}} \frac{\mathbf{K}_q \cdot \mathbf{K}_j}{\epsilon_q - \epsilon_j} - \sum_{\substack{q,j \\ j \neq q}} \frac{\mathbf{K}_j \cdot \mathbf{K}_q}{\epsilon_j - \epsilon_q} \quad (\text{A6b})$$

$$= 0. \quad (\text{A6c})$$

■

*Proposition 1.* The Gaudin Hamiltonians commute with the  $z$  component of the total angular momentum, i.e.,  $[H_q, L^z] = 0$ .

*Proof.* Follows directly from Theorem 1 and Lemma 1. ■

*Theorem 2.* For  $\gamma = -\frac{2}{g}$ , one can construct the BCS Hamiltonian with the Gaudin Hamiltonians [49],

$$H_{\text{BCS}} = -g \sum_q \epsilon_q H_q + g L^z + g (L^z)^2 + \text{const.} \quad (\text{A7})$$

*Proof.* It is

$$\sum_q \epsilon_q H_q = L^2 - \sum_q (\mathbf{K}_q^2 + \gamma \epsilon_q K_q^z), \quad (\text{A8})$$

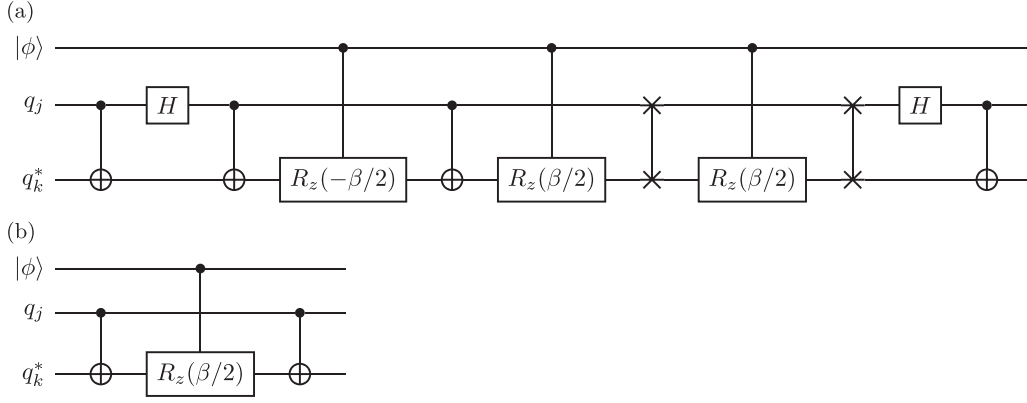


FIG. 7. Controlled versions of the (a) Heisenberg and (b) Ising gates from Figs. 3 and 2 and Eq. (14), with  $\beta = 4\alpha$ . The starred qubit indicates the central qubit (potentially after some swap operations) and  $|\phi\rangle$  is the control qubit.

since

$$2 \sum_{\substack{q,j \\ j \neq q}} \epsilon_q \frac{\mathbf{K}_q \cdot \mathbf{K}_j}{\epsilon_q - \epsilon_j} = \sum_{\substack{q,j \\ j \neq q}} \frac{\epsilon_q \mathbf{K}_q \cdot \mathbf{K}_j}{\epsilon_q - \epsilon_j} - \sum_{\substack{q,j \\ j \neq q}} \frac{\epsilon_q \mathbf{K}_j \cdot \mathbf{K}_q}{\epsilon_j - \epsilon_q} \quad (\text{A9a})$$

$$= \sum_{\substack{q,j \\ j \neq q}} \frac{\epsilon_q \mathbf{K}_q \cdot \mathbf{K}_j}{\epsilon_q - \epsilon_j} - \sum_{\substack{q,j \\ j \neq q}} \frac{\epsilon_j \mathbf{K}_q \cdot \mathbf{K}_j}{\epsilon_q - \epsilon_j} \quad (\text{A9b})$$

$$= \sum_{\substack{q,j \\ j \neq q}} \mathbf{K}_q \cdot \mathbf{K}_j. \quad (\text{A9c})$$

Splitting the  $L^2$ , we obtain

$$\sum_q \epsilon_q H_q = \frac{\gamma}{2} \left( - \sum_q 2\epsilon_q K_q^z + \frac{2}{\gamma} L^+ L^- \right) + L^z + (L^z)^2 - \sum_q K_q^2, \quad (\text{A10})$$

where we can identify the term in the parentheses with the BCS Hamiltonian. ■

*Proposition 2.* The Gaudin Hamiltonians and the  $z$  component of the total angular momentum commute with the BCS Hamiltonian, meaning  $[H_{\text{BCS}}, H_q] = 0$  and  $[H_{\text{BCS}}, L^z] = 0$ . All in all, all terms on the right-hand-side of Eq. (A7) commute with each other.

*Proof.* Follows directly from Theorems 1 and 2, and Proposition 1. ■

## APPENDIX B: MEAN-FIELD GROUND STATE

The mean-field ground state is obtained by inserting the approximation

$$c_{j\uparrow}^\dagger c_{j\downarrow}^\dagger c_{k\downarrow} c_{k\uparrow} \approx \langle c_{j\uparrow}^\dagger c_{j\downarrow}^\dagger \rangle \langle c_{k\downarrow} c_{k\uparrow} \rangle + \langle c_{j\uparrow}^\dagger c_{j\downarrow}^\dagger \rangle c_{k\downarrow} c_{k\uparrow} + c_{j\uparrow}^\dagger c_{j\downarrow}^\dagger \langle c_{k\downarrow} c_{k\uparrow} \rangle \quad (\text{B1a})$$

$$= \Delta_j^* \Delta_k + \Delta_j^* c_{k\downarrow} c_{k\uparrow} + c_{j\uparrow}^\dagger c_{j\downarrow}^\dagger \Delta_k \quad (\text{B1b})$$

in the Hamiltonian in Eq. (1) and diagonalizing the resulting Hamiltonian with a Bogoliubov transformation.  $\Delta_j = -\sum_k V_{jk} \langle c_{k\downarrow} c_{k\uparrow} \rangle$  is the superconducting gap for each energy level  $j$  where we replaced the constant coupling strength  $-g$

with  $V_{jk}$ . Without going into more detail [65], we present the resulting ground state,

$$|\text{BCS}\rangle = \prod_j (u_j - v_j K_j^+) |0\rangle, \quad (\text{B2})$$

with

$$|u_j|^2 = \frac{1}{2} \left( 1 + \frac{\epsilon_j}{E_j} \right), \quad (\text{B3})$$

$$|v_j|^2 = \frac{1}{2} \left( 1 - \frac{\epsilon_j}{E_j} \right), \quad (\text{B4})$$

$$\frac{v_j \Delta_j^*}{u_j} = E_j - \epsilon_j \in \mathbb{R}_+, \quad (\text{B5})$$

where we used the mean-field eigenvalues

$$E_j = \sqrt{\epsilon_j^2 + |\Delta_j|^2}. \quad (\text{B6})$$

The superconducting gaps must fulfill the system of gap equations,

$$\Delta_j = - \sum_k V_{jk} \frac{\Delta_k}{2E_k} \tanh \left( \frac{E_k}{2k_B T} \right), \quad (\text{B7})$$

for  $j \in \{1, \dots, n-1\}$ , where  $T$  is the temperature and  $k_B$  the Boltzmann constant. For  $V_{jk} = -g$ , the right-hand side of Eq. (B7) is independent of  $j$ , which implies

$$\Delta_j = \Delta, \quad (\text{B8})$$

and for  $\Delta \neq 0$ ,

$$\frac{2}{g} = \sum_k \frac{1}{E_k} \tanh \left( \frac{E_k}{2k_B T} \right). \quad (\text{B9})$$

## APPENDIX C: CONTROLLED TIME EVOLUTION

The algorithm described in Sec. V can be extended to a controlled version. Adding an additional control qubit  $|\phi\rangle$ , the time evolution shall be executed if  $|\phi\rangle = |1\rangle$  and not executed if  $|\phi\rangle = |0\rangle$ . This can be reached by controlling the single-qubit rotations. Figure 7 shows the Heisenberg and Ising gates accordingly. The structure of the whole circuit is similar to the one described in Fig. 4; however, the part containing the

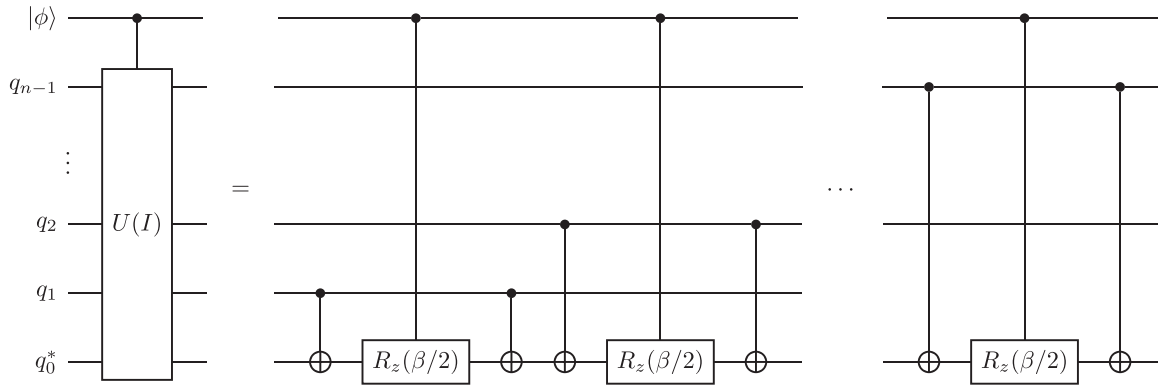


FIG. 8. Controlled version of the the gate in Fig. 4(d). The starred qubit indicates the central qubit and  $|\phi\rangle$  is the control qubit.

total angular momentum can be optimized to require fewer SWAP gates. First, one should swap the roles of the control and target qubit for the Ising-like terms  $U(I_q, t)$ , as shown

in Fig. 8; second, the additional controlled rotation  $e^{-i\frac{\zeta}{\hbar}g\sigma_q^z/2}$ , from the last term in Eq. (12b), should be executed directly after  $U(I_q, t)$ .

- [1] J. Preskill, Quantum computing in the NISQ era and beyond, *Quantum* **2**, 79 (2018).
- [2] F. Arute, K. Arya, R. Babbush, D. Bacon, J. C. Bardin, R. Barends, R. Biswas, S. Boixo, F. G. S. L. Brandao, D. A. Buell, B. Burkett, Y. Chen, Z. Chen, B. Chiaro, R. Collins, W. Courtney, A. Dunsworth, E. Farhi, B. Foxen, A. Fowler *et al.*, Quantum supremacy using a programmable superconducting processor, *Nature (London)* **574**, 505 (2019).
- [3] M. Mohseni, P. Read, H. Neven, S. Boixo, V. Denchev, R. Babbush, A. Fowler, V. Smelyanskiy, and J. Martinis, Commercialize quantum technologies in five years, *Nature (London)* **543**, 171 (2017).
- [4] A. Montanaro, Quantum algorithms: An overview, *npj Quantum Inf.* **2**, 15023 (2016).
- [5] P. W. Shor, Polynomial-time algorithms for prime factorization and discrete logarithms on a quantum computer, *SIAM Rev.* **41**, 303 (1999).
- [6] S. J. Lomonoca, Jr. and L. H. Kauffman, Quantum hidden subgroup problems: A mathematical perspective, [arXiv:quant-ph/0201095](https://arxiv.org/abs/0201095).
- [7] E. Farhi, J. Goldstone, and S. Gutmann, A quantum approximate optimization algorithm, [arXiv:1411.4028](https://arxiv.org/abs/1411.4028).
- [8] E. Farhi and A. W. Harrow, Quantum supremacy through the quantum approximate optimization algorithm, [arXiv:1602.07674](https://arxiv.org/abs/1602.07674).
- [9] S. Lloyd, Universal quantum simulators, *Science* **273**, 1073 (1996).
- [10] D. S. Abrams and S. Lloyd, Simulation of Many-Body Fermi Systems on a Universal Quantum Computer, *Phys. Rev. Lett.* **79**, 2586 (1997).
- [11] A. Aspuru-Guzik, A. D. Dutoi, P. J. Love, and M. Head-Gordon, Simulated quantum computation of molecular energies, *Science* **309**, 1704 (2005).
- [12] J. Haah, M. B. Hastings, R. Kothari, and G. H. Low, Quantum algorithm for simulating real time evolution of lattice Hamiltonians, *SIAM J. Comput.* **FOCS18–250** (2021).
- [13] M. B. Hastings, D. Wecker, B. Bauer, and M. Troyer, Improving quantum algorithms for quantum chemistry, *Quantum Inf. Comput.* **15**, 1 (2015).
- [14] G. Ortiz, J. E. Gubernatis, E. Knill, and R. Laflamme, Quantum algorithms for fermionic simulations, *Phys. Rev. A* **64**, 022319 (2001).
- [15] D. Wecker, M. B. Hastings, N. Wiebe, B. K. Clark, C. Nayak, and M. Troyer, Solving strongly correlated electron models on a quantum computer, *Phys. Rev. A* **92**, 062318 (2015).
- [16] D. Wecker, M. B. Hastings, and M. Troyer, Progress towards practical quantum variational algorithms, *Phys. Rev. A* **92**, 042303 (2015).
- [17] D. Wecker, B. Bauer, B. K. Clark, M. B. Hastings, and M. Troyer, Gate-count estimates for performing quantum chemistry on small quantum computers, *Phys. Rev. A* **90**, 022305 (2014).
- [18] R. P. Feynman, Simulating physics with computers, *Intl. J. Theor. Phys.* **21**, 467 (1982).
- [19] D. Gottesman, An introduction to quantum error correction and fault-tolerant quantum computation, [arXiv:0904.2557](https://arxiv.org/abs/0904.2557).
- [20] D. Aharonov and M. Ben-Or, Fault-tolerant quantum computation with constant error rate, *SIAM J. Comput.* **38**, 1207 (2008).
- [21] S. B. Bravyi and A. Y. Kitaev, Quantum codes on a lattice with boundary, [arXiv:quant-ph/9811052](https://arxiv.org/abs/quant-ph/9811052).
- [22] E. Dennis, A. Kitaev, A. Landahl, and J. Preskill, Topological quantum memory, *J. Math. Phys.* **43**, 4452 (2002).
- [23] A. G. Fowler, M. Mariantoni, J. M. Martinis, and A. N. Cleland, Surface codes: Towards practical large-scale quantum computation, *Phys. Rev. A* **86**, 032324 (2012).
- [24] P. W. Shor, Scheme for reducing decoherence in quantum computer memory, *Phys. Rev. A* **52**, R2493 (1995).
- [25] P. J. J. O'Malley, R. Babbush, I. D. Kivlichan, J. Romero, J. R. McClean, R. Barends, J. Kelly, P. Roushan, A. Tranter, N. Ding, B. Campbell, Y. Chen, Z. Chen, B. Chiaro, A. Dunsworth, A. G. Fowler, E. Jeffrey, E. Lucero, A. Megrant, J. Y. Mutus *et al.*, Scalable Quantum Simulation of Molecular Energies, *Phys. Rev. X* **6**, 031007 (2016).
- [26] A. Tranter, S. Sofia, J. Seeley, M. Kaicher, J. McClean, R. Babbush, P. V. Coveney, F. Mintert, F. Wilhelm, and P. J. Love, The Bravyi-Kitaev transformation: Properties and applications, *Intl. J. Quantum Chem.* **115**, 1431 (2015).

- [27] E. A. Yuzbashyan, B. L. Altshuler, V. B. Kuznetsov, and V. Z. Enolskii, Solution for the dynamics of the BCS and central spin problems, *J. Phys. A: Math. Gen.* **38**, 7831 (2005).
- [28] L. Childress, M. V. G. Dutt, J. M. Taylor, A. S. Zibrov, F. Jelezko, J. Wrachtrup, P. R. Hemmer, and M. D. Lukin, Coherent dynamics of coupled electron and nuclear spin qubits in diamond, *Science* **314**, 281 (2006).
- [29] P. Neumann, N. Mizuochi, F. Rempp, P. Hemmer, H. Watanabe, S. Yamasaki, V. Jacques, T. Gaebel, F. Jelezko, and J. Wrachtrup, Multipartite entanglement among single spins in diamond, *Science* **320**, 1326 (2008).
- [30] L. Jiang, J. S. Hodges, J. R. Maze, P. Maurer, J. M. Taylor, D. G. Cory, P. R. Hemmer, R. L. Walsworth, A. Yacoby, A. S. Zibrov, and M. D. Lukin, Repetitive readout of a single electronic spin via quantum logic with nuclear spin ancillae, *Science* **326**, 267 (2009).
- [31] M. V. G. Dutt, L. Childress, L. Jiang, E. Togan, J. Maze, F. Jelezko, A. S. Zibrov, P. R. Hemmer, and M. D. Lukin, Quantum register based on individual electronic and nuclear spin qubits in diamond, *Science* **316**, 1312 (2007).
- [32] M. Steiner, P. Neumann, J. Beck, F. Jelezko, and J. Wrachtrup, Universal enhancement of the optical readout fidelity of single electron spins at nitrogen-vacancy centers in diamond, *Phys. Rev. B* **81**, 035205 (2010).
- [33] B. Smeltzer, J. McIntyre, and L. Childress, Robust control of individual nuclear spins in diamond, *Phys. Rev. A* **80**, 050302(R) (2009).
- [34] G. Waldherr, Y. Wang, S. Zaiser, M. Jamali, T. Schulte-Herbrüggen, H. Abe, T. Ohshima, J. Isoya, J. F. Du, P. Neumann, and J. Wrachtrup, Quantum error correction in a solid-state hybrid spin register, *Nature (London)* **506**, 204 (2014).
- [35] F. Dolde, I. Jakobi, B. Naydenov, N. Zhao, S. Pezzagna, C. Trautmann, J. Meijer, P. Neumann, F. Jelezko, and J. Wrachtrup, Room-temperature entanglement between single defect spins in diamond, *Nat. Phys.* **9**, 139 (2013).
- [36] N. Kalb, P. C. Humphreys, J. J. Slim, and R. Hanson, Dephasing mechanisms of diamond-based nuclear-spin memories for quantum networks, *Phys. Rev. A* **97**, 062330 (2018).
- [37] S. Pezzagna and J. Meijer, Quantum computer based on color centers in diamond, *Appl. Phys. Rev.* **8**, 011308 (2021).
- [38] J. Wrachtrup, S. Y. Kilin, and A. P. Nizovtsev, Quantum computation using the  $^{13}\text{C}$  nuclear spins near the single NV defect center in diamond, *Opt. Spectrosc.* **91**, 429 (2001).
- [39] M. W. Doherty, N. B. Manson, P. Delaney, F. Jelezko, J. Wrachtrup, and L. C. Hollenberg, The nitrogen-vacancy colour center in diamond, *Phys. Rep.* **528**, 1 (2013).
- [40] L. Robledo, L. Childress, H. Bernien, B. Hensen, P. F. A. Alkemade, and R. Hanson, High-fidelity projective read-out of a solid-state spin quantum register, *Nature (London)* **477**, 574 (2011).
- [41] R. Finsterhoelzl and G. Burkard, Benchmarking quantum error-correcting codes on quasi-linear and central-spin processors, *Quantum Sci. Technol.* **8**, 015013 (2023).
- [42] V. Vorobyov, J. Javadzade, M. Joliffe, F. Kaiser, and J. Wrachtrup, Addressing single nuclear spins quantum memories by a central electron spin, *Appl. Magnet. Reson.* **53**, 1317 (2022).
- [43] J. Bardeen, L. N. Cooper, and J. R. Schrieffer, Theory of superconductivity, *Phys. Rev.* **108**, 1175 (1957).
- [44] J. von Delft and D. Ralph, Spectroscopy of discrete energy levels in ultrasmall metallic grains, *Phys. Rep.* **345**, 61 (2001).
- [45] J. von Delft and F. Braun, Quantum mesoscopic phenomena and mesoscopic devices in microelectronics; Superconductivity in ultrasmall grains introduction to richardson's exact solution, *Nato Science Series* **559**, 361 (2000).
- [46] J. Dukelsky, S. Pittel, and G. Sierra, Colloquium: Exactly solvable Richardson-Gaudin models for many-body quantum systems, *Rev. Mod. Phys.* **76**, 643 (2004).
- [47] P. Anderson, Theory of dirty superconductors, *J. Phys. Chem. Solids* **11**, 26 (1959).
- [48] F. Braun and J. von Delft, Fixed- $N$  Superconductivity: The Crossover from the Bulk to the Few-Electron Limit, *Phys. Rev. Lett.* **81**, 4712 (1998).
- [49] M. Cambiaggio, A. Rivas, and M. Saraceno, Integrability of the pairing Hamiltonian, *Nucl. Phys. A* **624**, 157 (1997).
- [50] E. K. Sklyanin, Separation of variables: New trends, *Prog. Theor. Phys. Suppl.* **118**, 35 (1995).
- [51] V. B. Kuznetsov, Quadrics on real Riemannian spaces of constant curvature: Separation of variables and connection with Gaudin magnet, *J. Math. Phys.* **33**, 3240 (1992).
- [52] E. K. Sklyanin, Separation of variables in the Gaudin model, *J. Sov. Math.* **47**, 2473 (1989).
- [53] N. Fröhling, F. B. Anders, and M. Glazov, Nuclear spin noise in the central spin model, *Phys. Rev. B* **97**, 195311 (2018).
- [54] E. Frenkel, Affine algebras, Langlands duality and Bethe ansatz, [arXiv:q-alg/9506003](https://arxiv.org/abs/q-alg/9506003).
- [55] L.-A. Wu, M. S. Byrd, and D. A. Lidar, Polynomial-Time Simulation of Pairing Models on a Quantum Computer, *Phys. Rev. Lett.* **89**, 057904 (2002).
- [56] K. M. Svore, M. B. Hastings, and M. H. Freedman, Faster phase estimation, *Quantum Inf. Comput.* **14**, 306 (2014).
- [57] G. Burkard, Recipes for the digital quantum simulation of lattice spin systems, [arXiv:2209.07918](https://arxiv.org/abs/2209.07918).
- [58] M. Suzuki, General theory of fractal path integrals with applications to many-body theories and statistical physics, *J. Math. Phys.* **32**, 400 (1991).
- [59] N. Wiebe, D. Berry, P. Høyer, and B. C. Sanders, Higher order decompositions of ordered operator exponentials, *J. Phys. A: Math. Theor.* **43**, 065203 (2010).
- [60] A. Papageorgiou and C. Zhang, On the efficiency of quantum algorithms for Hamiltonian simulation, *Quantum Inf. Process.* **11**, 541 (2012).
- [61] S. Raesi, N. Wiebe, and B. C. Sanders, Quantum-circuit design for efficient simulations of many-body quantum dynamics, *New J. Phys.* **14**, 103017 (2012).
- [62] M. R. Geller, The universe as a nonlinear quantum simulation, [arXiv:2112.09005](https://arxiv.org/abs/2112.09005).
- [63] M. Heyl, Dynamical quantum phase transitions: A review, *Rep. Prog. Phys.* **81**, 054001 (2018).
- [64] Y. Adamov, I. V. Gornyi, and A. D. Mirlin, Loschmidt echo and Lyapunov exponent in a quantum disordered system, *Phys. Rev. E* **67**, 056217 (2003).
- [65] M. Tinkham, *Introduction to Superconductivity*, 2nd ed. (McGraw-Hill, New York, 1996).
- [66] Qiskit, [github.com/Qiskit](https://github.com/Qiskit), version 0.34.0 (unpublished).

- [67] A. Mitra, Quantum quench dynamics, *Annu. Rev. Condens. Matter Phys.* **9**, 245 (2018).
- [68] P. Calabrese, F. H. L. Essler, and M. Fagotti, Quantum Quench in the Transverse-Field Ising Chain, *Phys. Rev. Lett.* **106**, 227203 (2011).
- [69] A. M. Childs, D. Maslov, Y. Nam, N. J. Ross, and Y. Su, Toward the first quantum simulation with quantum speedup, *Proc. Natl. Acad. Sci.* **115**, 9456 (2018).
- [70] D. W. Berry, A. M. Childs, R. Cleve, R. Kothari, and R. D. Somma, Simulating Hamiltonian Dynamics with a Truncated Taylor Series, *Phys. Rev. Lett.* **114**, 090502 (2015).
- [71] H. Perrin, T. Scoquart, A. Shnirman, J. Schmalian, and K. Snizhko, Mitigating crosstalk errors by randomized compiling: Simulation of the BCS model on a superconducting quantum computer, [arXiv:2305.02345](https://arxiv.org/abs/2305.02345).